ornl

OAK RIDGE
NATIONAL
LABORATORY

MARTIN MARIETTA

ORNL/TM-11481

MARTIN MARIETTA ENERGY SYSTEMS LIBRARIES

3 4456 0314823 4

Reaction Rate Distributions and Related Data in the FNS Phase II Experiments:

Comparison of Measured and Calculated Data

R. T. Santoro
R. G. Alsmiller, Jr.
J. M. Barnes

OAK RIDGE NATIONAL LABORATORY
CENTRAL RESEARCH LIBRARY
CIRCULATION SECTION
4500N ROOM 175
LIBRARY LOAN COPY
DO NOT TRANSFER TO ANOTHER PERSON
If you wish someone else to see this report, send in name with report and the library will arrange a loan.

OPERATED BY
MARTIN MARIETTA ENERGY SYSTEMS, INC.
FOR THE UNITED STATES
DEPARTMENT OF ENERGY

This report has been [illegible]

Available to [illegible] Technical Information [illegible] from (615) 576 [illegible]

Available to the [illegible] Department of [illegible]

This report was prepared as an account of work sponsored by an agency of the United States Government. Neither the United States Government nor any agency thereof, nor any of their employees, makes any warranty, express or implied, or assumes any legal liability or responsibility for the accuracy, completeness, or usefulness of any information, apparatus, product, or process disclosed, or represents that its use would not infringe privately owned rights. Reference herein to any specific commercial product, process, or service by trade name, trademark, manufacturer, or otherwise, does not necessarily constitute or imply its endorsement, recommendation, or favoring by the United States Government or any agency thereof. The views and opinions of authors expressed herein do not necessarily state or reflect those of the United States Government or any agency thereof.

ORNL/TM-11481

Engineering Physics and Mathematics Division

REACTION RATE DISTRIBUTIONS AND RELATED DATA IN THE FNS PHASE II EXPERIMENTS:

COMPARISON OF MEASURED AND CALCULATED DATA

R. T. Santoro
R. G. Alsmiller, Jr.
J. M. Barnes

DATE PUBLISHED - July 1990

Prepared by the
OAK RIDGE NATIONAL LABORATORY
Oak Ridge, Tennessee 37831
operated by
MARTIN MARIETTA ENERGY SYSTEMS, INC.
for the
U. S. DEPARTMENT OF ENERGY
under Contract No. DE-AC05-84OR21400

MARTIN MARIETTA ENERGY SYSTEMS LIBRARIES

3 4456 0314823 4

CONTENTS

	Page
LIST OF TABLES	v
LIST OF FIGURES	vii
ABSTRACT	ix
1. INTRODUCTION	1
2. DETAILS OF THE MEASUREMENTS AND CALCULATIONS	3
3. DISCUSSION OF RESULTS	7
3.1 SOURCE SPECTRUM COMPARISON	7
3.2 COMPARISON OF MEASURED AND CALCULATED ACTIVATION DATA	8
3.3 TRITIUM PRODUCTION RATES IN THE Li_2O ASSEMBLY	10
3.4 CONCLUSIONS	11
REFERENCES	25

LIST OF TABLES

Page

1. Composition of Materials Used in the Calculations 15

2. 53-Neutron Group Energy Structure and Tritium Breeding Cross Sections 16

3. Activation Cross Sections 17

4. C/E Values for the $^{27}Al(n,\alpha)$ Reaction as a Function of Detector Location 18

5. C/E Values for the $^{58}Ni(n,p)$ Reaction as a Function of Detector Location 19

6. C/E Values for the $^{93}Nb(n,2n)$ Reaction as a Function of Detector Location 20

7. C/E Values for the $^{197}Au(n,2n)$ Reaction as a Function of Detector Location. 21

8. C/E Values for the $^{58}Ni(n,2n)$ Reaction as a Function of Detector Location 22

9. Tritium Production in ^{6}Li in the Phase II Li_2O Assembly 23

10. Tritium Production in ^{7}Li in the Phase II Li_2O Assembly 24

LIST OF FIGURES

Page

1. Schematic of the Experimental Assembly 12

2. Comparison of the Measured and Calculated Neutron Source Spectrum on the Mid-Plane of the Experimental Assembly at the Face of the Li_2O Assembly 13

3. Locations of the Activation Foil Packets 14

ABSTRACT

Neutronics parameters including the source neutron spectrum, activation rates, and the tritium breeding in the Li_2O test zone of the Phase II experiment performed at JAERI have been calculated using the Monte Carlo code MORSE using ENDF/B-V transport and reaction cross-sections. Favorable comparisons between the measured and calculated results have been achieved for the $^{27}Al(n,\alpha)$, $^{58}Ni(n,p)$, $^{93}Nb(n,2n)$, and $^{197}Au(n,2n)$ reactions. Calculated $^{58}Ni(n,2n)$ and $^{197}Au(n,\gamma)$ reactions did not agree with measured values within 10-40%. For the Ni reaction the differences may be due to poor data in the ORACT files while discrepancies for the Au data may be due to unknown quantities of hydrogen rich epoxy used to coat the Li_2CO_3 blocks used in the test assembly walls. The calculated tritium breeding in the Li_2O agreed with experimental values within ±10% for ^6Li and ±15-20% for ^7Li.

1. INTRODUCTION

Integral experiments are being carried out at the Fusion Neutron Source (FNS) at the Japan Atomic Energy Research Institute (JAERI) to measure the tritium breeding ratios (TPR) and related neutronics data in prototypic fusion reactor blanket assemblies. This effort is being done as part of the joint fusion neutronics program between the U.S. Department of Energy and JAERI. Detailed and comprehensive experiments are performed to obtain neutronics parameters for validating and benchmarking the radiation transport codes and cross-section data that are expected to be used in blanket design calculations.[1-10]

In this paper, neutron induced reaction rates and related data including the tritium production along the axis of a Li_2O blanket mock-up calculated using the Monte Carlo code MORSE-CG[11] are compared with measured data for the Phase II experimental assembly. [9-10] The activation data were obtained on the river surfaces of the experimental assembly. In-system for activation measurements and analyses were also carried out and are also reported in Ref. 9 and 10. Details of the assembly, methods of calculation, and data used to estimate the spatial dependence of the activation rates for the $^{27}Al(n,\alpha)$, $^{58}Ni(n,2n)$, $^{58}Ni(n,p)$, $^{93}Nb(n,2n)$, $^{197}Au(n,2n)$, and $^{197}Au(n,\gamma)$ reactions are described in Sect. 2. Comparisons of the calculated and measured reaction rates and and ditional data are presented and compared in Sect. 3.

2. DETAILS OF THE MEASUREMENTS AND CALCULATIONS

The primary purpose of the Phase II experiments is the determination of the tritium production rate (TPR) in a lithium-oxide (Li_2O) assembly having characteristics similar to those expected to be found in the breeding modules of a fusion reactor blank A midplane view of the experimental assembly is shown in Fig. 1. The system consists of a hollow rectangular parallelepiped whose major axis is coincident with the deuteron beam from the FNS accelerator. The walls of the assembly are constructed of lithium-carbonate (Li_2CO_3) blocks with a thin layer of aluminum lining the internal cavity and with sheets of polyethylene between the Li_2 $C0_3$ blocks and a Li_20 tritium breeding blanket experimental assembly and aluminum covering the external surfaces. A 60-cm-thick Li_2O blanket mock-up is located inside the Li_2CO_3 assembly opposite a rotating tritiated-titanium target that is mounted on the terminus of the deuteron beam flight tube. All of the components of the experimental system were modeled for these calculations using the combinatorial geometry (CG) subroutines of the MORSE code. The composition of the materials used in the analysis are given in Table 1.

Neutrons are produced in the rotating target assembly by the reactions of 350-keV deutrons in tritiated-titanium via the fusion reaction

$$D + T \rightarrow n + {}^4He + 17.6 \text{ MeV}. \qquad (1)$$

The probability that a deutron of energy E_d = 350 KeV reacts while slowing down in a distance dx in a target is

$$P = N_t \int_0^{E_d} \sigma / (dE/dx) \qquad (2)$$

where σ is the microscopic cross-section for the D-T reaction, N_t is the number of tritium atoms per cm^3, and dE/dx is the stopping power for deutrons in titanium-tritide. When the cross-section is given as a differential angular cross-section, P is the probability for neutron emission per unit solid angle. Equation 2 was evaluated using the methods described in Ref. 12. The emitted neutron distribution was binned into a multigroup energy format corresponding to that used in the radiation transport calculations.

The Monte Carlo calculations were performed using different neutron source biasing depending on the locations of the activation foils being analyzed. The activation rates in foils positioned on and nearby the face of the Li_2O assembly were obtained by directing 90% of the source neutrons into a cone having a polar angle of 45 degrees about the deuteron beam axis. For analysis of reactions on the side walls and behind the target, the biasing was such that 90% of the source neutrons were directed into the polar angular interval between 45 and 180 degrees. In both cases, the remaining 10% of the neutrons were directed into all other polar angles and uniform azimuthal neutron emission was assumed in all cases. The neutron flux was determined using next-flight estimation and convoluted with the cross-sections for the reaction to obtain the activation rates. Russian roulette and particle splitting were used to reduce the variance in the neutron flux.

The radiation transport was accomplished using a 53-neutron energy group cross-section library obtained by collapsing the VITAMIN-E 174-neutron group VITAMIN-E data[13]. The VITAMIN-E library (ENDF/B-V) was created as a general purpose cross-section data set for

fusion and fission reactor neutronics analysis problems. The broad group library was produced with the ANISN[14] code using the calculated forward emitted neutron energy-angle distribution from the target as the weighting function. The angular dependence of the cross-sections for all nuclei was approximated using a P_3 Legendre expansion. The energy boundaries of the broad group library and tritium breeding cross sections are given in Table 2.

The activation cross-sections[15] (excluding the $^{197}Au(n,\gamma)$ reaction) are summarized in Table 3.

3. DISCUSSION OF RESULTS

3.1 SOURCE SPECTRUM COMPARISON

To judge the validity of the neutron energy-angle distribution used in the sampling procedure in the Monte Carlo calculations and to assess the impact on this distribution of the modeling of the rotating target assembly, the neutron spectrum at the mid-plane of the Li_2O assembly was calculated and compared with measured data. The comparison is shown in Fig. 2. The solid curve is the calculated differential neutron spectrum obtained from the MORSE code for neutrons with energies above 2.5-MeV and the points are the measured data above 1.0-MeV. The calculated spectrum was smoothed using a typical NE-213 liquid scintillator response function given by

$$R_n = \sqrt{150 + 400/E_n} \tag{3}$$

where R_n is the full-width at half-maximum (in percent) of the detector response to neutrons of energy E_n. The numerical coefficients in Eq. 3 were determined by trial and error to obtain a best fit to the measured spectrum about the 14.1 MeV peak of the measured spectrum. These trials were necessary since the response data for the detector used in the measurement were not available at the time these calculations were made. The calculated spectrum above 2.5-MeV generally agrees very well with the measured data. Based on these results, it can be assumed that any differences that arise between the measured and calculated activation data are due to reasons other than the calculated neutron distribution. Any

differences can, therefore, be attributed to transport and activation reaction cross-sections, the calculational model geometry, material compositions, or the measured data.

3.2 COMPARISON OF MEASURED AND CALCULATED ACTIVATION DATA

The activation reactions were measured at numerous locations inside the cavity and walls of the experimental assembly.[9-10] The approximate locations of activation foil packets at which comparisons are reported in this paper are shown in Figs. 3a,b. The predominant number of measurements were made for foils located in the mid-plane of the experimental assembly as shown in Fig. 3a. The activation foil locations on the face of the Li_2O assembly are shown in Fig. 3b.

Table 4 compares the ratio of the calculated to measured (C/E) results for the $^{27}Al(n,\alpha)^{24}Na$ (E_{th} = 2.96 MeV) activation reaction as a function of the foil packet location. Listed in the table are the actual foil positions measured relative to the face of the rotating target assembly (x=y=z=0). The C/E results obtained in this work are compared with results reported by the JAERI staff[1] and data reported in Ref. 5. The column labeled "Ratio" is the ratio of the C/E values from the ORNL calculations to those obtained at JAERI. The calculated $^{27}Al(n,\alpha)$ activation is in good agreement with the measured results and those obtained at JAERI. The ORNL values range from a low C/E value of 0.88 to a high value of 1.11 with good agreement between measurement and calculation over the face of the Li_2O breeding assembly. Less favorable C/E results are observed for foils located at the corners of the assembly.

The C/E values for the $^{58}Ni(n,p)$ (E_{th} = 7.95 MeV), $^{93}Nb(n,2n)$ (E_{th} = 8.94-MeV), and the $^{197}Au(n,2n)$ (E_{th} = 8.12 MeV) activation reactions are summarized in Tables 5 to 7,

respectively, and are compared with the C/E results obtained at JAERI using the high energy threshold activation reaction cross-sections measured by Ikeda[16]. The calculated results reported here using cross-sections from the ORACT library (Ref. 15) are in excellent agreement with the measured results and also the C/E values obtained using Ikeda's data. Nakagawa (Ref. 3) reports C/E values obtained using ENDF/B-IV ^{93}Nb(n,2n) reaction data that are systematically larger than the values given in Table 6. The ORACT (ENDF/B-V) and Ikeda cross-sections lead to considerably improved results. The largest discrepancies between measured and calculated activations were observed for the ^{58}Ni(n,2n) and ^{197}Au(n,γ) reactions. The C/E values for the ^{58}Ni(n,2n) reaction are summarized in Table 8. The calculated activation obtained using the ORACT data files is, except in a few cases, lower than the measured data by nearly a factor of 2. Correspondingly, the C/E is also systematically smaller by a factor of two or more than the C/E results reported by the JAERI analysts using Ikeda's data. The discrepancy is most probably due to poor cross-section data for this reaction in the ORACT library.

The ^{197}Au(n,γ) activation data calculated at ORNL were considerably lower than the measured data. This reaction is sensitive to low energy neutrons. The lithium-carbonate blocks used to construct the experimental assembly were coated with a hydrogen-loaded epoxy paint. This fact was not known at the time these calculations were made so the composition for the Li_2CO_3 used in the calculations does not account for the hydrogen or other elements in the epoxy. While not including the epoxy composition has little effect on high energy neutron transport, the omission may have serious consequences on the calculation of the ^{197}Au(n,γ) reaction which is predominately sensitive to thermal and epithermal energy neutrons.

3.3 TRITIUM PRODUCTION RATES IN THE Li_2O ASSEMBLY

The tritium production as a function of depth along the central axis of the Li_2O assembly was calculated using collision density estimation. The estimator is given by

$$T = (\Sigma_i/\Sigma_T) \times neutron\ weight,\ i=6,7$$

where Σ_i is the cross section for the production of tritium from neutron reactions with ^6Li (i = 6) or ^7Li (i = 7) and Σ_T is the total cross section in Li_2O. The ratio of these probabilities is multiplied by the weight of the neutron prior to initiation of the reaction. The spatial distribution of the tritium production was obtained by dividing the Li_2O into 16 axial intervals with the interval boundaries selected to bracket the location of the detectors used in the measurements. The Monte Carlo was run using a neutron source population sufficiently large to achieve approximately ±10% standard deviation in the estimated tritium production at the face of the Li_2O. The measured an calculated data are normalized to one source neutron and the ^6Li and ^7Li nuclide densities in the Li_2O.

The measured and calculated tritium production from the reactions of the source neutrons with ^6Li nuclei in the Li_2O are summarized in Table 9. The calculated TPR is in good agreement with the measured data[6,17,18] at all locations except the first and last intervals where the calculated data are low by nominally 14-20%. The Monte Carlo calculation reproduces the measurement at the remaining locations within 10% or better. The results obtained here show considerable improvement over previously calculated TPR data for the Phase I experiment[18]. The better comparisons indicated in Table 9 can be attributed, in part, to the improved experimental geometry used in the Phase II measurements.[5,7]

The tritium production as a function of depth in the Li_2O from the reactions of the source neutron with ^7Li nuclei are compared in Table 10. The calculated TPR is in fair agreement with the measured data. The calculation under predicts the measurement at the front of the Li_2O assembly by about 25% but agrees to within 10-15% in the remaining intervals with the exception of a few points where the calculated TPR values deviate from the expected exponential drop-off with depth.

3.4 CONCLUSIONS

The Monte Carlo code MORSE in combination with ENDF/B-V transport and ORACT activation cross-sections does a favorable job of reproducing the measured spectra, activation, and tritium production for the Phase II experiment assembly. The activation calculations have clearly identified a problem in the ORACT $^{58}Ni(n,p)$ activation cross section that corroborates the observations made by Nakagawa (Ref. 3). The agreement achieved between the measured and calculated TPR is acceptable and further supports previous observations on the effectiveness of Monte Carlo calculational methods for analysis of the tritium production for the FNS experiments and for their potential in fusion reactor design studies.

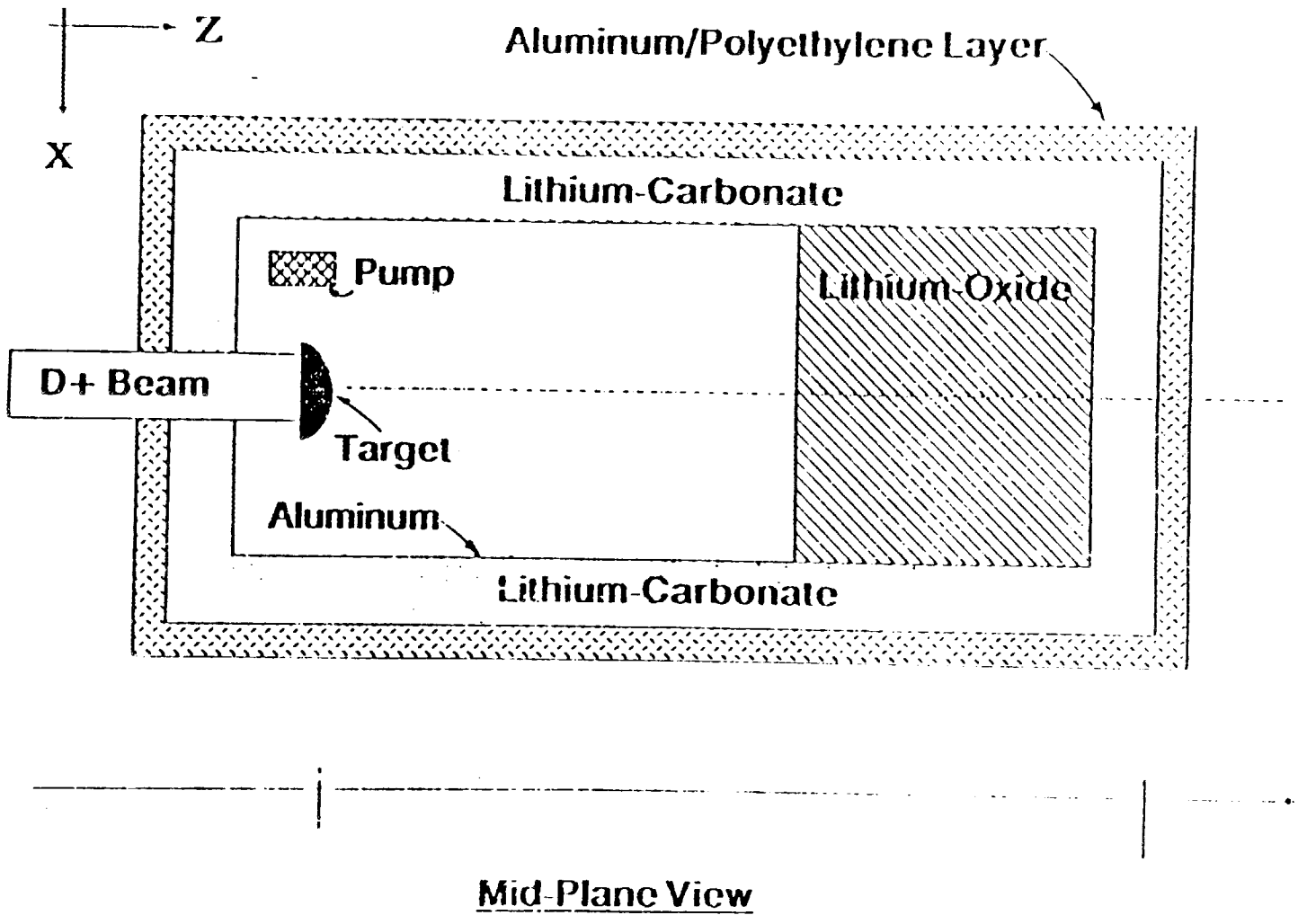

Fig. 1. Schematic of the experimental assembly.

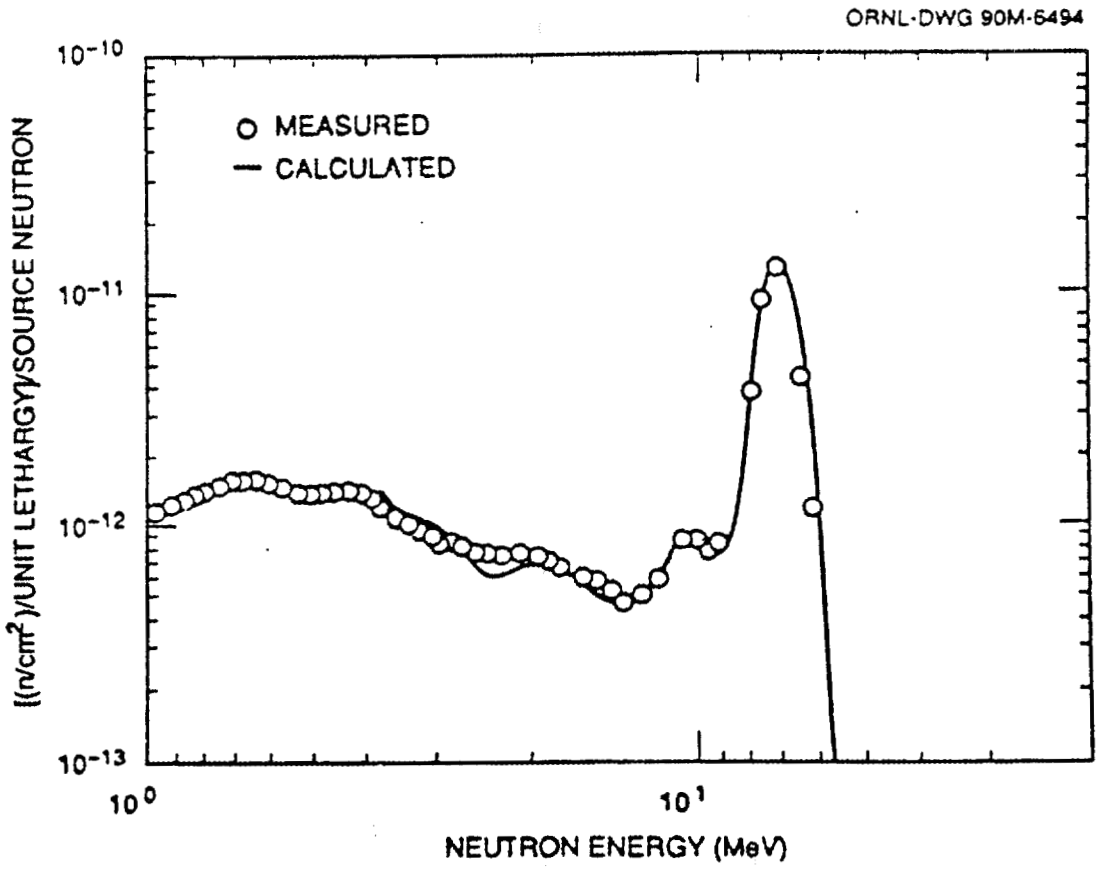

Fig. 2. Comparison of the measured and calculated neutron source spectrum on the mid-plane of the experimental assembly at the face of the Li_2O assembly.

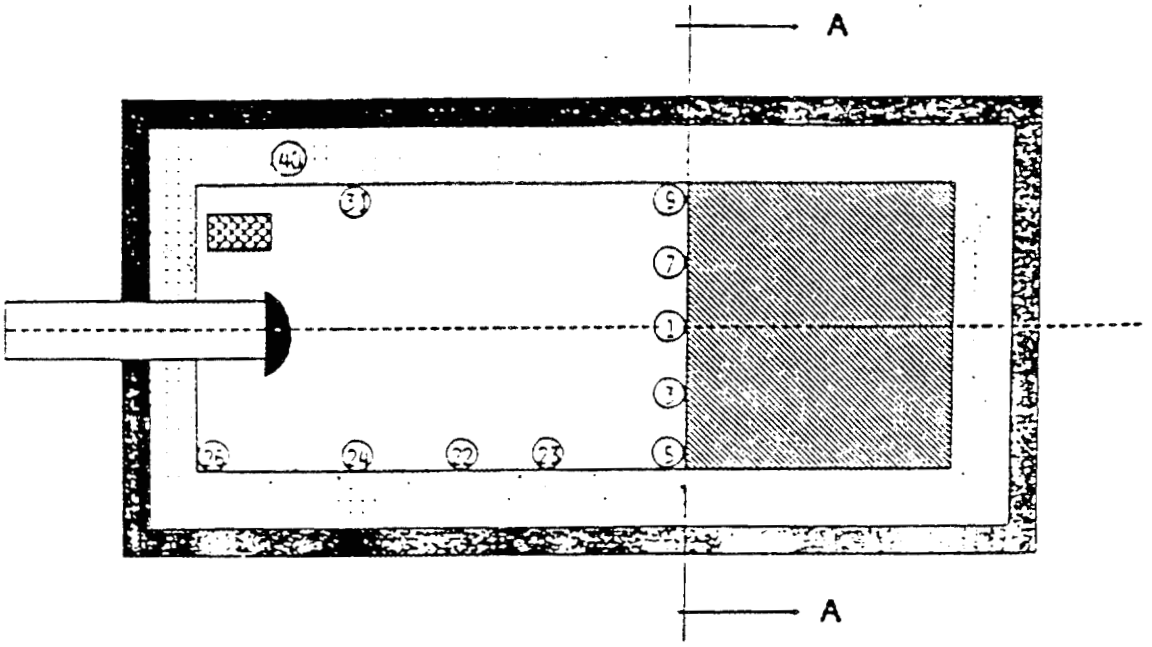

(a)

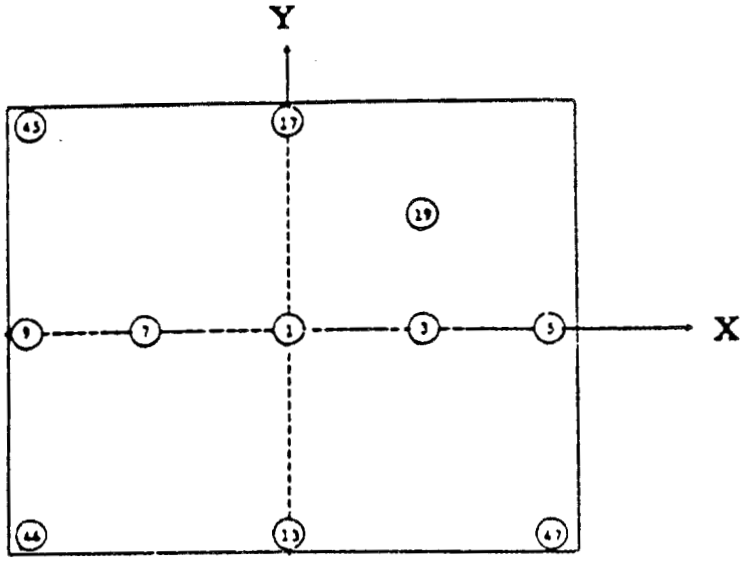

Section A-A

(b)

Fig. 3a-b. Locations of the activation foil packets.

Table 1. Composition of materials used in the calculations (atoms/cm-barn).

Element	Li_2O	Li_2CO_3	Poly	Concrete	SS-304
H			7.979-2	7.974-3	
^6Li	4.242-3*	2.580-3			
^7Li	5.293-2	3.182-2			
C		1.716-2	3.953-2	5.904-4	
O	2.858-3	5.163-2		4.315-2	
Na				7.859-4	
Mg				3.824-4	
Al				2.637-3	
Si				1.481-2	
K				5.288-4	
Ca				2.564-3	
Cr		2.564-4			1.768-2
Mn		2.235-4			1.765-2
Fe		9.224-4			6.020-2
Ni		1.126-4			7.828-3
	H_2O	Al	$Cu+H_2O$	Cu	
H	6.691-2		2.810-2		
O	3.346-2		1.405-2		
Al		6.004-2			
Cu			8.493-2	8.460-2	

*Read as 4.242×10^{-3}

Table 2. 53-Neutron group energy structure and tritium breeding cross-sections.

Group	Upper Energy (eV)	Tritium Breeding in ^{6}Li (barns)	Tritium Breeding in ^{7}Li (barns)	Group	Upper Energy (eV)	Tritium Breeding in ^{6}Li (barns)
1	17.33+6	0.0193	0.2468	28	6.081+5	0.3386
2	15.68+6	0.0239	0.2869	29	4.978+5	0.4881
3	14.92+6	0.0246	0.2929	30	3.688+5	0.9891
4	14.55+6	0.0253	0.2985	31	2.985+5	1.5271
5	14.19+6	0.0266	0.3039	32	2.927+5	2.4440
6	13.84+6	0.0266	0.3091	33	1.832+5	0.9060
7	13.30+6	0.0273	0.3149	34	1.111+5	0.6553
8	12.84+6	0.0294	0.3304	35	6.737+4	0.7194
9	12.21+6	0.0323	0.3419	36	4.087+4	0.8693
10	11.05+6	0.0359	0.3542	37	2.479+4	0.9860
11	10.00+6	0.0402	0.3636	38	2.359+4	1.1017
12	9.05+6	0.0454	0.3707	39	1.503+4	1.3824
13	8.19+6	0.0506	0.3751	40	4.119+3	1.7608
14	7.41+6	0.0598	0.3714	41	5.531+3	2.2521
15	6.06+6	0.0752	0.2525	42	3.354+3	2.8847
16	4.97+6	0.0956	0.0753	43	2.035+3	3.7109
17	4.07+6	0.1122	0.0158	44	1.234+3	4.7769
18	3.68+6	0.1436	0.0010	45	7.485+2	6.1240
19	2.73+6	0.1925		46	4.450+2	7.8654
20	2.37+6	0.2025		47	2.754+2	10.102
21	2.31+6	0.2051		48	1.670+2	12.978
22	2.21+6	0.2102		49	1.013+2	16.660
23	1.65+6	0.2141		50	6.144+1	21.404
24	1.35+6	0.2465		51	3.726+1	31.860
25	8.63+6	0.2484		52	1.067+1	76.377
26	8.21+6	0.2584		53	4.139-1	526.5
27	7.43+6	0.2843			1.000-5	

Table 3. Activation cross-sections (barns).

Group No.	$^{27}Al(n,\alpha)$	$^{58}Ni(n,2n)$	$^{58}Ni(n,p)$	$^{93}Nb(n,2n)$	$^{197}Au(n,2n)$
1	7.031-02*	5.571-02	1.675-01	4.444-01	1.654-00
2	1.120-01	4.557-02	2.454-01	4.983-01	2.162-00
3	1.166-01	3.911-02	2.762-01	4.979-01	2.170-00
4	1.206-01	3.256-02	3.066-01	4.976-01	2.170-00
5	1.243-01	2.614-02	3.370-01	4.973-01	2.166-00
6	1.276-01	1.961-02	3.720-01	4.969-01	2.131-00
7	1.282-01	1.239-02	4.118-01	4.939-01	2.086-00
8	1.248-01	1.882-04	5.174-01	4.663-01	1.961-00
9	1.162-01		5.686-01	3.972-01	1.861-00
10	9.977-02		6.126-01	2.065-01	1.488-00
11	8.161-02		6.290-01	3.407-02	7.757-01
12	5.912-02		6.350-01		1.972-01
13	3.550-02		6.360-01		7.518-04
14	1.153-02		6.152-01		
15	6.891-04		5.720-01		
16			4.192-01		
17			3.929-01		
18			2.184-01		
19			1.086-01		
20			8.032-02		
21			7.226-02		
22			3.968-02		
23			1.324-02		
24			3.221-03		
25			5.911-04		
26			4.358-04		
27			1.626-04		
28			3.646-07		

* Read as 7.031×10^{-2}

Table 4. C/E values for the $^{27}Al(n,\alpha)$ reaction as a function of detector location.

Detector Number	Coordinates (cm) x (mm)	y	z	C/E (ORNL)	C/E (JAERI)	Ratio*
1	0	0	0	1.01	1.00	1.01
3	210	0	0	1.03	1.02	1.01
5	420	0	0	0.94	0.96	0.98
7	-210	0	0	1.01	1.05	0.96
9	-420	0	0	0.92	1.03	0.89
13	0	-420	0	0.92	1.02	0.90
17	0	420	0	0.99	1.04	0.95
19	210	210	0	1.11	N/A**	----
22	433	0	205	0.99	0.98	1.01
23	433	0	412	0.99	1.01	0.98
24	433	0	811	0.96	1.05	0.91
26	433	0	1030	1.06	1.00	1.06
31	-433	0	618	0.94	1.02	0.92
40	-623	0	821	0.90	1.00	0.90
45	-420	420	0	0.88	N/A	----
46	-420	-420	0	0.88	N/A	----
47	420	-420	0	0.88	N/A	----

* Ratio = [C/E(ORNL)]/[C/E(JAERI)].
** Not available.

Table 5. C/E values for the $^{58}Ni(n,p)$ reaction as a function of detector location.

Detector Number	Coordinates (cm) x (mm)	y	z	C/E (ORNL)	C/E (JAERI)	Ratio*
1	0	0	0	1.07	1.05	1.02
3	210	0	0	1.13	1.00	1.13
5	420	0	0	1.01	1.05	0.96
7	-210	0	0	1.14	1.10	1.04
9	-420	0	0	0.98	1.08	0.91
13	0	-420	0	1.01	1.10	0.92
17	0	420	0	0.99	0.98	1.01
19	210	210	0	0.93	N/A**	----
22	433	0	205	1.04	1.01	1.03
23	433	0	412	1.10	1.05	1.05
24	433	0	811	1.05	1.13	0.93
26	433	0	1030	1.03	1.02	1.01
31	-433	0	618	0.97	1.08	0.90
40	-623	0	821	0.86	0.94	0.91
45	-420	420	0	1.09	N/A	----
46	-420	-420	0	1.00	N/A	----
47	420	-420	0	0.99	N/A	----

*Ratio = [C/E(ORNL)]/[C/E(JAERI)].
** Not available.

Table 6. C/E values for the $^{93}Nb(n,2n)$ reaction as a function of detector location.

Detector Number	Coordinates (cm) x (mm)	y	z	C/E (ORNL)	C/E (JAERI)	Ratio*
1	0	0	0	1.09	1.01	1.08
3	210	0	0	1.02	1.00	1.02
5	420	0	0	0.98	0.99	0.99
7	-210	0	0	1.02	1.05	0.97
9	-420	0	0	1.00	1.09	0.92
13	0	-420	0	0.97	1.02	0.95
17	0	420	0	1.00	1.05	0.95
19	210	210	0	1.07	N/A**	----
22	433	0	205	1.01	1.02	0.99
23	433	0	412	1.03	1.03	1.00
24	433	0	811	1.04	1.07	0.97
26	433	0	1030	1.23	1.23	1.00
31	-433	0	618	1.01	1.10	0.92
40	-623	0	821	1.00	0.98	1.02
45	-420	420	0	0.87	N/A	----
46	-420	-420	0	0.88	N/A	----
47	420	-420	0	0.97	N/A	----

* Ratio = [C/E(ORNL)]/[C/E(JAERI)].
** Not available.

Table 7. C/E values for the $^{197}Au(n,2n)$ reaction as a function of detector location.

Detector Number	Coordinates (cm) x (mm)	y	z	C/E (ORNL)	C/E (JAERI)	Ratio*
1	0	0	0	0.98	0.96	1.02
3	210	0	0	0.97	0.96	1.01
5	420	0	0	0.93	0.95	0.98
7	-210	0	0	0.97	0.98	0.99
9	-420	0	0	0.91	1.01	0.90
13	0	-420	0	0.86	0.95	0.91
17	0	420	0	0.91	0.95	0.96
19	210	210	0	1.04	N/A**	----
22	433	0	205	0.96	0.94	1.02
23	433	0	412	0.96	0.98	0.98
24	433	0	811	0.93	1.02	0.91
26	433	0	1030	1.24	N/A	----
31	-433	0	618	0.94	1.01	0.93
40	-623	0	821	N/A	N/A	----
45	-420	420	0	0.88	N/A	----
46	-420	-420	0	0.84	N/A	----
47	420	-420	0	0.93	N/A	----

* Ratio = [C/E(ORNL)]/[C/E(JAERI)].
** Not available.

Table 8. C/E values for the $^{58}Ni(n,2n)$ reaction as a function of detector location.

Detector Number	Coordinates (cm) x	y	z	C/E (ORNL)	C/E (JAERI)	Ratio*
	(mm)					
1	0	0	0	0.67	1.04	0.64
3	210	0	0	0.66	1.00	0.66
5	420	0	0	0.66	0.96	0.69
7	-210	0	0	0.66	1.10	0.60
9	-420	0	0	0.68	1.11	0.61
13	0	-420	0	0.60	1.10	0.55
17	0	420	0	0.66	1.03	0.64
19	210	210	0	0.63	N/A	----
22	433	0	205	0.67	1.01	0.66
23	433	0	412	0.70	1.05	0.67
24	433	0	811	0.84	1.13	0.74
26	433	0	1030	0.99	0.94	1.05
31	-433	0	618	0.85	1.08	0.79
40	-623	0	821	1.13	1.12	1.01
45	-420	420	0	0.55	N/A	----
46	-420	-420	0	0.66	N/A	----
47	420	-420	0	0.59	N/A	----

* Ratio = [C/E(ORNL)]/[C/E(JAERI)].
** Not available.

Table 9. Tritium production in ^6Li in the phase II Li_2O assembly.

	Distance	Calculated TPR[a]	Measured TPR[b]	C/E
1	1.15	7.89(-29)[c]	9.16(-29)	0.86
2	3.45	7.22(-29)	7.64(-29)	0.95
3	5.75	6.47(-29)	7.08(-29)	0.91
4	8.05	6.03(-29)	6.76-(29)	0.89
5	10.35	5.49(-29)	6.08-(29)	0.95
6	12.65	5.48(-29)	5.50(-29)	0.99
7	14.95	5.22(-29)	5.02(-29)	1.04
8	17.84	4.89(-29)	4.58(-29)	1.07
9	22.69	3.81(-29)	3.91(-29)	0.97
10	27.60	3.31(-29)	3.29(-29)	1.01
11	32.51	2.75(-29)	2.75(-29)	1.00
12	37.42	2.21(-29)	2.26(-29)	0.98
13	42.89	1.78(-29)	1.82(-29)	0.98
14	47.65	1.41(-29)	1.48(-29)	0.95
15	52.41	1.19(-29)	1.24(-29)	0.95
16	57.17	9.10(-30)	1.21(-29)	0.81

a. TPR/[^6Li Atom • Source Neutron].
b. TPR/[^6Li Atom • Source Neutron].
c. Read as 7.89×10^{-29}.

Table 10. Tritium production in ^7Li in the phase II Li_2O assembly.

	Distance	Calculated TPR[a]	Measured TPR[b]	C/E
1	1.15	3.79(-30)[c]	5.00(-30)	0.75
2	3.45	3.11(-30)	4.21(-30)	0.74
3	5.75	2.97(-30)	3.30(-30)	0.90
4	8.05	2.41(-30)	2.97(-30)	0.81
5	10.35	2.19(-30)	2.23(-30)	0.98
6	12.65	1.98(-30)	2.23(-30)	0.89
7	14.95	1.57(-30)	2.00(-30)	0.79
8	17.84	1.39(-30)	1.42(-30)	0.98
9	22.69	1.05(-30)	1.06(-30)	0.99
10	27.60	7.41(-31)	7.71(-31)	0.96
11	32.51	5.21(-31)	5.10(-31)	1.02
12	37.42	3.46(-31)	3.11(-31)	1.11
13	42.89	2.13(-31)	2.10(-31)	1.01
14	47.65	1.82(-31)	1.73(-31)	1.05
15	52.41	1.36(-31)	1.63(-31)	0.84
16	57.17	8.05(-32)	9.52(-32)	0.85

a. TPR/[^{7}Li Atom • Source Neutron].
b. TPR/[^{7}Li Atom • Source Neutron].
c. Read as 3.79×10^{-30}.

REFERENCES

1. T. Nakamura and M. Abdou, "Summary of Recent Results from the JAERI/US Fusion Neutronics Phase I Experiments", Fusion Technol., 10 (1986) 541.
2. M. Youssef, et al., "Analysis and Intercomparison for Phase I Fusion Integral Experiments at the FNS Facility", Fusion Technol., 10 (1986) 549.
3. M. Nakagawa, et al., "Analysis of Neutronic Parameters Measured in Phase II Experiments of the JAERI/US Collaborative Program on Fusion Neutronics. PartI: Source Characteristics and Reaction Rate Distributions", Fusion Eng. and Des. 9 (1989) 315.
4. M.Y. Youssef, et al., "Analysis of Neutronics Parameters Measured in Phase II Experiments of the JAERI/US Collaborative Program on Fusion Neutronics. Part II: Tritium Production and In-System Spectra", Fusion Eng. and Des., 9 (1989) 323.
5. M. Nakagawa, et al., "JAERI/US Collaborative Program on Fusion Blanket Neutronics: Analysis of Phase IIA and IIB Experiments", JAER-M-89-154, Japan Atomic Energy Research Institute, October 1989.
6. Y. Oyama, et al., "Phase IIA and IIB Experiments of JAERI/USDOE Collaborative Program on Fusion Blanket Neutronics", JAERI-M-89-215 (Part I) and JAERI-M-89-215 (Part II), Japan Atomic Energy Research Institute, December 1989.
7. M. Youssef, et al., "USDOE/JAERI Collaborative Program on Fusion Neutronics: Phase IIA and IIB Fusion Intergral Experiments, The US Analysis", UCLA-ENG-90-14, FNT-31, University of California at Los Angeles, December 1989.
8. M. Youssef, et al., "Comparative Analysis for Phase IIA and IIB Experiments of the US/JAERI Collaborative Program on Fusion Blanket Neutronics", Fusion Technology, 15, 1287-1292 (1989).

9. Y. Ikeda, et al., "Neutron Source and Field Characteristics Measurement for JAERI/USDOE Phase II Experiments on Fusion Blanket Neutronics", Fusion Engr. & Design, 9, 303-308 (1989).

10. Y. Ikeda, et al., "Determination of Neutron Spectrum in D-T Fusion Field by Foil Activation Technique", Fusion Technology, 15 1297-1292 (1989).

11. M.B. Emmett, "The MORSE Monte Carlo Radiation Transport Code System", ORNL-4744, Oak Ridge National Laboratory (1975).

12. R.T. Santoro, J.M. Barnes, J.D. Drischler, and R.G. Alsmiller, Jr., "Multigroup Energy-Angle Distributions for Neutrons From the ^{4}He Reaction (E_d=100-400 keV)", ORNL/TM-9251, Oak Ridge National Laboratory (1984).

13. C.R. Weisbin, et al., "VITAMIN-E: An ENDF/B Multigroup Cross-Section Library for LMFBR Core and Shield, LWR Shield, Dosimetry, and Fusion Blanket Technology", ORNL-5505, Oak Ridge National Laboratory (1979).

14. W.W. Engle, Jr., "A Users Manual for ANISN, A One-Dimensional Discrete Ordinates Transport code with Anisotropic Scattering", K-1693, Oak Ridge National Laboratory (1967).

15. R.T. Santoro, J.E. White, and J.D. Drischler, "ORACT, a 174-Neutron Group Activation Cross Section Library for Fusion and Fission Reactor Studies", ORNL/TM-9203, Oak Ridge National Laboratory (1984).

16. Y. Ikeda, et al., "Measurement of High Threshold Activation Cross Sections for 13.5 to 15 MeV Neutrons", Proc. Intl. Conf. on Nuclear Data for Basic and Applied Science, Santa Fe, NM (1985).

17. Y. Oyama, et al., "Experimental Results for the Phase II of the JAERI/USDOE Collaborative Program on Fusion Blankets", First International Symposium on Fusion Nuclear Technology, Tokyo, Japan. See also Fusion Engineering and Design, 9 309-313 (1989).

18. R.T. Santoro, R.G. Alsmiller, Jr., J.M. Barnes, and T.A. Gabriel, "Comparison of Calculated Results with Experimental Data for the Tritium Production Rates in a Li20 Assembly", ORNL/TM-11181, Oak Ridge National Laboratory (1989). Accepted for publication in Nuclear Science and Engineering.

ORNL/TM-11481
Dist. Cat. UC-

INTERNAL DISTRIBUTION

1. F. S. Alsmiller
2-6. R. G. Alsmiller, Jr.
7. B. R. Appleton
8-12. J. M. Barnes
13. L. A. Berry
14. T. A. Gabriel
15. D. T. Ingersoll
16. R. A. Lillie
17. F. C. Maienschein
18. R. W. Peelle
19. V. Protopopescu
20. R. W. Roussin
21. M. W. Rosenthal
22-26. R. T. Santoro
27. T. E. Shannon
28. EPMD Reports Office
29-30. Laboratory Records Laboratory
31. Laboratory Records ORNL-RC
32. Document Reference Section
33. Central Research Library
34. ORNL Patent Section

EXTERNAL DISTRIBUTION

35. S. E. Berk, Division of Development and Technology, Office of Fusion Energy, ER-532, U.S. Department of Energy, Washington, D.C. 20545
36. J. J. Dorning, Department of Nuclear Engineering and Engineering Physics, Thornton Hall, University of Virginia, Charlottesville, Virginia 22901
37. Y. Gohar, Argonne National Laboratory, 9700 S. Cass Avenue, Argonne, Illinois 60439
38. R. M. Haralick, Department of Electrical Engineering, University of Washington, Seattle, Washington 98195
39. James E. Leiss, 13013 Chestnut Oak Drive, Gaithersburg, Maryland 20878
40. Neville Moray, Department of Mechanical and Industrial Engineering, University of Illinois, 1206 West Green Street, Urbana, Illinois 61801
41. Dr. Yasushi Seki, Japan Atomic Energy Research Institute, Tokai-mura, Ibaraki-ken, Japan
42. Mary F. Wheeler, Mathematics Department, University of Houston, 4800 Calhoun, Houston, Texas 77204-3476
43. Thermonuclear Library, Japan Atomic Energy Research Institute, Tokai, Naka, Ibaraki, Japan
44. Office of the Assistant Manager for Energy Research and Development, Department of Energy, Oak Ridge Operations, P.O. Box 2001, Oak Ridge, TN 37831

45-54. Office of Scientific and Technical Information, P.O. Box 62, Oak Ridge, TN 37830